The Effect of Thermal Aging and Addition of CeOx, NbOx, and SbOx on the Structure of Dispersed VOx in Low-Loaded Anatase-Supported

THE JOURNAL OF PHYSICAL CHEMISTRY C
A JOURNAL OF THE AMERICAN CHEMICAL SOCIETY

pubs.acs.org/JPCC

Article

The Effect of Thermal Aging and Addition of CeO_x, NbO_x, and SbO_x on the Structure of Dispersed VO_x in Low-Loaded Anatase-Supported Vanadia Catalysts

Alexander Nellessen, Iliana-Maria Stergiou, Theocharis Kentri, Roberta Villamaina, Anna Martinelli, Andreas Schaefer, Per-Anders Carlsson,* and Soghomon Boghosian*

Cite This: J. Phys. Chem. C 2026, 130, 4096−4108

Read Online

ACCESS | Metrics & More | Article Recommendations | Supporting Information

ABSTRACT: In situ vibrational spectroscopy (Raman, FTIR) is used at temperatures of 120−430 °C under oxidative dehydration conditions to study the effect of CeO_x, NbO_x, and SbO_x modifiers, as well as the effect of thermal aging, on the structural and configurational properties of titania(anatase)-supported vanadia catalysts. The study pertains to catalysts with low vanadium coverage (i.e., ∼0.5 V nm^{-2}) and an M/V molar ratio (M = Ce, Nb, Sb) equal to one. The dispersed $(VO_x)_n$ phase consists of three species with distinct configurations: a majority Species-I with an O═V(−O−Ti)$_3$ configuration (V═O terminal mode at 1024−1027 cm^{-1}) followed by Species-II with an O═V(−O−Ti)$_4$ configuration (V═O terminal mode at 1014−1016 cm^{-1}) and a minority Species-III with an $(O═V)_2(-O-Ti)_x$ configuration (symmetric stretching mode at ∼1000 cm^{-1}). Lowering of the temperature in the 430−120 °C range results in reversible temperature-dependent structural transformations. First, in the 430−250 °C range, a Species-II to Species-I transformation takes place, followed by a Species-I to Species-III transformation at lower temperatures. Modifying the VO_x/TiO_2(anatase) catalysts with CeO_x, NbO_x, or SbO_x results in the increased presence of Species-I at the expense of Species-II. Thermal aging of the studied catalysts at 580 °C for 100 h gives rise to structural transformation of the anatase carrier, resulting in an increased presence of (101) facets and severe lowering of the specific surface area, thereby causing an increase in Species-I at the expense of Species-II and in the formation of V−O−V and/or V−O−M linkages. The results are deemed important for gaining insight into the structure and the behavior of anatase-supported vanadia catalysts.

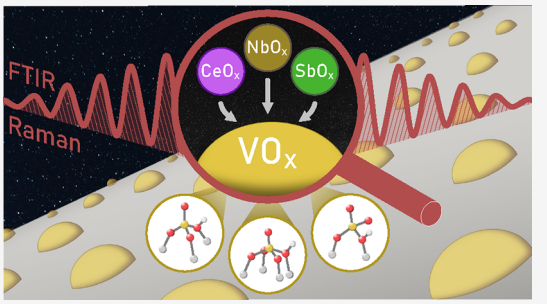

INTRODUCTION

Many industrial chemical processes use titania-supported vanadium oxide (VO_x/TiO_2) as heterogeneous catalysts. Well-known examples of applications are the oxidation of sulfur dioxide to sulfur trioxide in the production of sulfuric acid,[1] the oxidative dehydrogenation of light alkanes,[2,3] and the selective catalytic reduction of NO_x with ammonia (NH_3-SCR)[4] for emission control. Anatase TiO_2 is widely used as a support for the catalytic phase, thanks to its high surface area and suitable active phase−support interaction, resulting in enhanced catalytic activity and stability of the dispersed active phase.[5−7]

Fundamental interest has been focused on the identification of the configurational characteristics of the dispersed VO_x species.[8−11] For this purpose, the use of Raman and Fourier-transform infrared (FTIR) spectroscopy applied under in situ conditions has been shown to be a strong combination. A combined Raman−FTIR in situ spectroscopic study[12] has shown that, for low vanadium coverage (≤0.74 V atoms per nm^2, V nm^{-2}), the dispersed VO_x phase comprises three distinct species/units that occur in isolated/monomeric form, as shown in Figure 1. Species-I is the predominant species, with a mono-oxo distorted tetrahedral configuration (CN_V = 4); two other species occur in minority, Species-II with a mono-oxo distorted octahedral configuration (CN_V = 5), and Species-III with a dioxo configuration.[12] The terms "tetrahedral-like with CN_V = 4" and "octahedral-like with CN_V = 5" are used to indicate that the proposed configurations are not perfect but rather distorted. Species-I possesses a distorted tetrahedral VO_4 configuration with one O atom offered by titania and a proton on a V−O−Ti bridge (bridge-bond protonation, V−OH−Ti). The higher wavenumber for Species-I is justified by the lower coordination number for the V atom. DFT studies have shown that the configurations of dispersed VO_x sites on anatase are facet-dependent and that at low coverage, i.e., below 2 V nm^{-2}, the prevalent tetrahedral

Received: December 19, 2025
Revised: February 25, 2026
Accepted: February 26, 2026
Published: March 5, 2026

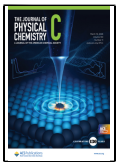

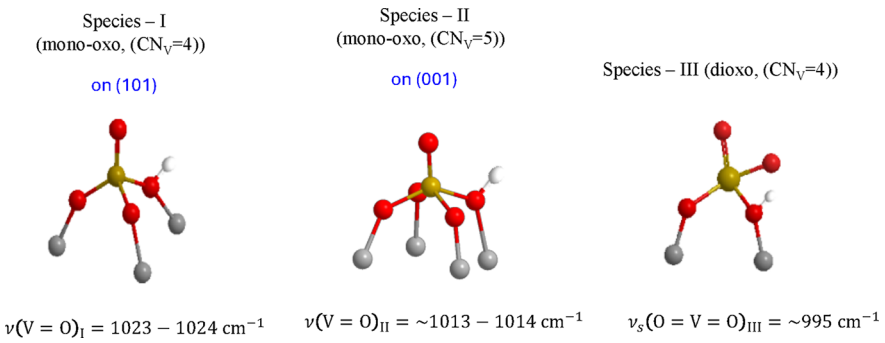

Figure 1. Proposed structural models for the distinct dispersed VO_x Species-I, -II, and -III.[12] Atom colors: gold, V; red, O; gray, Ti; and white, H.

Table 1. Sample Characteristics Including Target Composition (in wt %), SSA, and Vanadium Surface Density

	composition/wt %				SSA/$m^2\ g^{-1}$		V surface density/V nm^{-2}	
sample	V	Ce	Nb	Sb	fresh	aged	fresh	aged
TiO_2 (DT51-D)					88	47		
V/Ti	0.35				93	30	0.4	1.4
V−Ce/Ti	0.35	0.96			83	53	0.5	0.8
V−Nb/Ti	0.35		0.64		94	35	0.4	1.2
V−Sb/Ti	0.35			0.84	89	33	0.5	1.2

mono-oxo Species-I occurs on the majority (101) facet, and the less abundant octahedral-like mono-oxo Species-II occurs on the minority (001) facet.[10,13] Although experimental in situ spectroscopic studies are often performed under dehydrated conditions, it must be noted that water is an ubiquitous molecule and that fully dehydrated dispersed VO_x on titania occurs only under extreme conditions, such as ultrahigh vacuum, ensuring absolute absence of water.[11,13−15] Therefore, the state of a catalyst under dehydrated feed conditions should rather be described as hydroxylated, since the dissociative adsorption of water would result in OH formation, e.g., by protonation of V−O−Ti anchoring bonds.[15] Such hydroxylated VO_x species dispersed on TiO_2 facets are proposed as stable sites based on theoretical and density functional theory (DFT) calculations.[9,10,13,14] Experimental and theoretical molecular dynamics (MD) and DFT studies concluded that water molecules hydrolyze V−O−Ti bonds through dissociative adsorption.[13−15] Hence, a progressive hydroxylation is observed as the temperature decreases. Additionally, DFT studies showed that at low coverages ($\leq$0.8 V nm^{-2}), the hydroxyl formation on the titania surface is energetically favored.[10]

The relative presence of the three species is found to be temperature-dependent, leading to reversible structural transformations. When lowering the temperature, e.g., from 430 to 250 °C, water molecules retained by the surface mediate transformations from Species-II to Species-I. Further lowering of the temperature, from 250 to 175 and then to 120 °C, results in a transformation of Species-I into Species-III. The mechanism of the structural transformations is the hydrolysis of the V−O−Ti sites, thereby resulting in surface hydroxylation.[12]

Depending on the intended application, several challenges must be addressed, including initial activity, thermal deactivation, and sensitivity to poisoning. Vanadium oxide particles are known to be sensitive to thermal stress, thereby undergoing aggregation as well as inducing transformation processes of the TiO_2 support.[16−18] Consequently, the development of VO_x/TiO_2 catalysts has been focused on optimizing the catalytic properties, enhancing thermal stability, and improving chemical resistance through the incorporation of metal oxides. For instance, previous studies have shown that the incorporation of cerium improves the low-temperature activity (200−250 °C),[19−22] while modification with niobium oxides has been shown to preserve the activity after thermal stress.[23−25] The Sb-modification has also shown benefits, including a significant catalyst activation after thermal treatment.[23,26−28]

The aim of this study is 2-fold, viz.: (i) to elucidate how addition of CeO_x, NbO_x, and SbO_x to the VO_x/TiO_2 system modifies the configurational characteristics of dispersed VO_x species for the as-prepared samples, and (ii) how thermal aging affects these VO_x species using the as-prepared samples as references. To this end, in situ Raman and FTIR spectroscopies (the latter in the overtone region) have been applied under oxidative dehydrated feed conditions to study catalyst samples with very low V coverage (i.e., ~0.5 V nm^{-2}). This is to ensure, as much as possible, the occurrence of VO_x sites in isolated form and enable the distinction of spectroscopic signatures caused by structurally different species.

MATERIALS AND METHODS

Sample Preparation

The catalyst samples were prepared by incipient wetness impregnation of DT-51D TiO_2 (Tronox plc, 99 wt % anatase) using a vanadyl oxalate solution (GfE GmbH). The modified samples were prepared by coimpregnation with cerium(III) nitrate hexahydrate (Sigma-Aldrich), niobium(V) oxalate solution (Sigma-Aldrich), or antimony-(III) acetate solution (Sigma-Aldrich) as precursors. The respective loading was chosen to obtain an equimolar ratio of vanadium and the modifier atom. The target vanadium loading was 0.35 wt % with 0.96 wt % cerium, 0.64 wt % niobium, or 0.84 wt % antimony. After impregnation, the powder samples were calcined in stationary air at 500 °C for 1 h. The resulting powder samples are referred to as 'fresh'. Thermal aging was performed by heating a portion of the fresh samples for an additional 100 h at 580 °C in static air. The resulting samples are labeled as 'aged'.

https://doi.org/10.1021/acs.jpcc.5c08604
J. Phys. Chem. C 2026, 130, 4096−4108

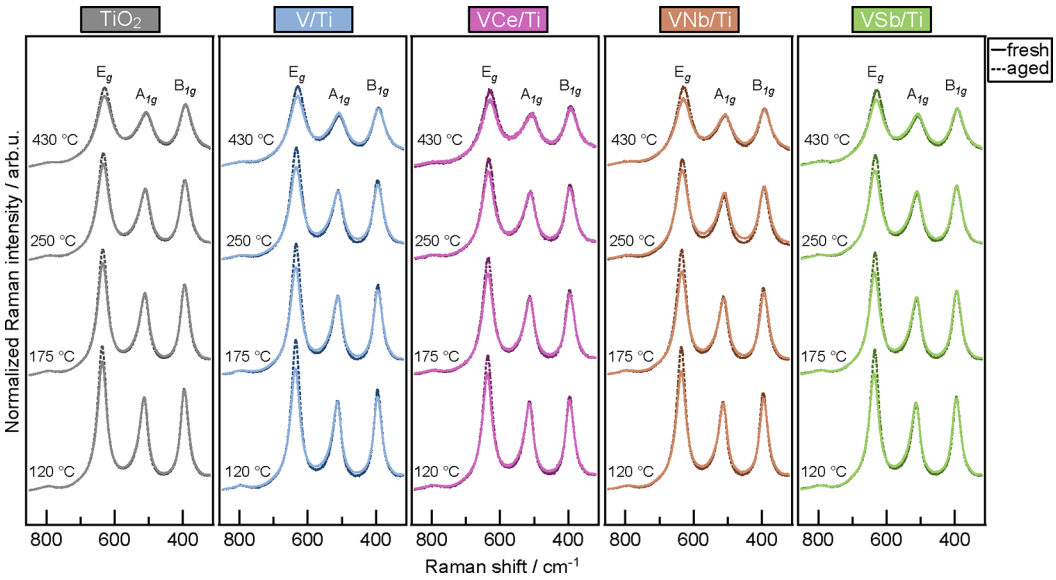

Figure 2. Sequential in situ Raman spectra obtained for bare TiO_2 support, unmodified VO_x/TiO_2, as well as for modified VO_x/TiO_2 samples before and after the aging procedure under flowing 20% O_2/He, as indicated in each panel. Recording parameters: laser wavelength, λ = 491.5 nm; laser power, w = 10 mW; time constant, τ = 1.2 s; and spectral slit width, ssw = 7 cm^{-1}.

Sample Characterization

The specific surface area (SSA) of fresh and aged catalyst samples was measured by N_2 physisorption using a Micromeritics Tristar 3000 instrument at −196 °C and the Brunauer−Emmett−Teller (BET) model. Before each measurement, about 200 mg of sample was dried at 250 °C in a nitrogen flow for 6 h.

The SSA was used as a basis for calculating the vanadium surface density, n_s, expressed in V nm^{-2}, according to

$$n_s\ (\mathrm{V\ nm^{-2}}) = \frac{x_V \times N_A}{M_V \times \mathrm{SSA} \times 10^{18}\ (\mathrm{nm^2/m^2})} \quad (1)$$

in which x_V (g/g) is the vanadium content, N_A is the Avogadro number (6.022×10^{23} mol^{-1}), M_V is the molecular mass of vanadium (50.94 g mol^{-1}), and SSA is given in m^2 g^{-1}. The V surface density determined for the fresh samples was in the 0.4−0.5 V nm^{-2} range. After the samples had been subjected to thermal aging, the V surface densities were found to be in the range of 0.8−1.4 V nm^{-2}, due to the correspondingly commensurate reduction of the SSA, in each case. Table 1 summarizes the properties of the catalyst samples.

The in situ Raman spectra of the catalyst samples were recorded using a homemade optical Raman cell, which has previously been described in detail.[2,29] Typically, 130−140 mg of a powdered sample from each catalyst was pressed into a pellet using a hydraulic press at 25 kN load. The pellet was mounted on the sample holder of the cell and heated for 1 h at 430 °C in dry flowing (30 mL/min) 20% O_2/He feed gas (He 99.999% and O_2 99.999% from L' Air Liquide). The 491.5 nm (cyan) line of a Cobolt Calypso DPSS laser, operated at a power of ∼10 mW, was used for exciting the Raman spectra. In order to limit the irradiance, the incoming beam was slightly defocused by a cylindrical lens, thereby resulting in an ∼2 mm^2 spot size on the sample. A horizontal scattering plane with right-angle scattered radiation collection was set as the optical geometry. The scattered light was analyzed with a 1403 Spex 0.85 m double monochromator and detected by a −20 °C cooled RCA photomultiplier tube interfaced with the LabSpec software. The spectra were recorded under dehydrated feed conditions starting from a temperature of 430 °C. Temperature was subsequently lowered to 250, 175, and 120 °C under a continuous flow of the dry O_2/He feed gas, and the in situ Raman spectra were collected after 1 h of sample treatment at each temperature. Finally, a replicate spectrum was recorded at 430 °C to confirm restoration of the catalyst structure. The spectral resolution was set to 7 cm^{-1}. To obtain a high signal-to-noise ratio, a slow scan speed with 1.2 s of photon counting per point at increments of 0.25 cm^{-1} was implemented. The Raman spectra obtained were subjected to normalization, as previously described[30,31] to account for the so-called "path length" effect of colored samples.

The in situ FTIR spectra in steady state were recorded with a Nicolet 6700 FTIR spectrometer, equipped with a KBr beam splitter and an MCTB detector, and a Spectra Tech DRIFT in situ cell. The measurement protocol was identical to that implemented for the in situ Raman measurements. First, each sample was treated for 1 h at 430 °C under a flow of dry 20% O_2/He gas (at a flow of 30 mL/min) before recording the in situ FTIR spectrum at 430 °C. The spectral resolution was 4 cm^{-1}, and 64 scans were averaged for each spectrum. Then, the temperature was lowered in steps according to the sequence 430 → 250 → 175 → 120 °C, with spectra recorded at steady-state conditions at each temperature. Again, a replicate spectrum was recorded at 430 °C to validate the restoration of the catalyst structure.

RESULTS AND DISCUSSION

Effect of Modifiers and Thermal Aging on the Titania Structure

Figure 2 shows the Raman spectra in the 350−850 cm^{-1} spectral region, which exhibits vibrational modes of the anatase phase of TiO_2. The structure of TiO_2 in the anatase form is tetragonal and belongs to the space group D_{4h}^{19} (I_4/amd).[32,33] According to the factor group analysis, the expected optical modes in anatase span the irreducible representation $1A_{1g} + 1A_{2u} + 2B_{1g} + 1B_{2u} + 3E_g + 2E_u$, of which the A_{1g}, B_{1g}, and E_g modes are Raman-active. Typical wavenumbers for these modes, based on experimental measurements as well as calculations, are 144 cm^{-1} (E_g), 197 cm^{-1} (E_g), 399 cm^{-1} (B_{1g}), 513 cm^{-1} (A_{1g}), 519 cm^{-1} (B_{1g}), and 639 cm^{-1} (E_g).[32,34] The recorded Raman spectrum for the bare TiO_2 support at 430 °C exhibits the expected Raman-active modes, with clear features at 391 cm^{-1} (B_{1g}), 509 cm^{-1} (A_{1g}), and 630 cm^{-1} (E_g). The 144 cm^{-1} E_g mode is by far the strongest in the anatase Raman spectrum but has not been included in Figure 2 to display changes and differences of the modes observed in the 300−850 cm^{-1} spectrum more clearly. Notably, the 509 cm^{-1} feature also includes the B_{1g} mode in the low-frequency wing of the main A_{1g} mode, as discussed in detail by Giarola et

https://doi.org/10.1021/acs.jpcc.5c08604
J. Phys. Chem. C 2026, 130, 4096−4108

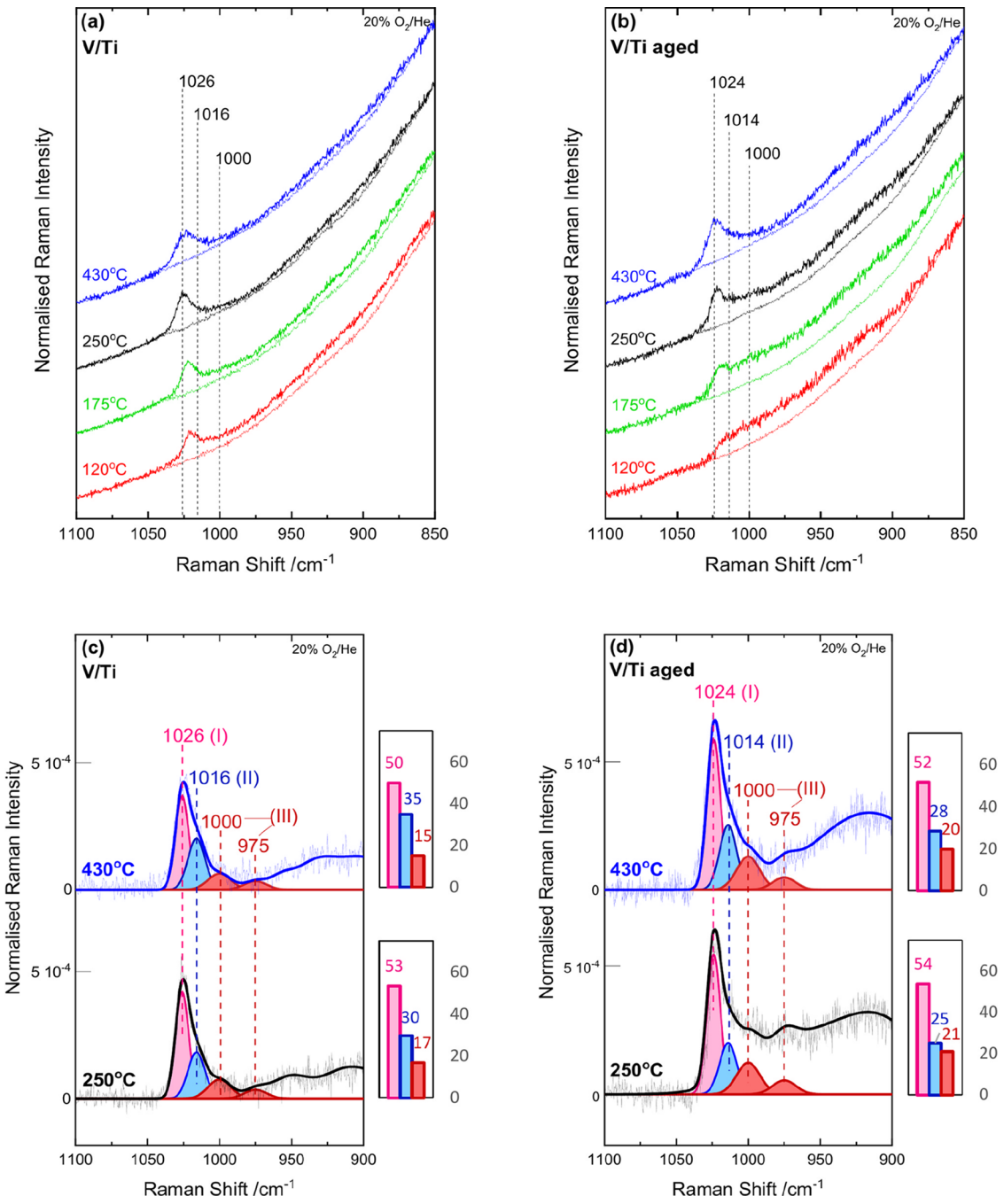

Figure 3. Sequential (430 → 250 → 175 → 120 °C) in situ Raman spectra obtained for unmodified VO_x/TiO_2 before (a) and after (b) the aging procedure under flowing 20% O_2/He at temperatures, as indicated by each spectrum. The spectra obtained for bare TiO_2 (DT51-D) are also shown as reference background under each spectrum. Peak analysis of in situ Raman spectra of V/Ti before (c) and after (d) aging after subtraction of the corresponding TiO_2 (DT51-D) backgrounds at 430 and 250 °C. Recording parameters: see Figure 2 caption.

al. using polarized Raman spectroscopy.[34] An additional spectral feature is observed at 795 cm^{-1}, which is assigned to a second-order vibration of the B_{1g} mode at 396 cm^{-1}.[35] The spectra shown in Figure 2 are recorded at a sequence of decreasing temperatures. Upon sequential cooling, the observed bands slightly blue shift (to 396, 513, and 637 cm^{-1}) as a consequence of lattice contraction. The addition of vanadium and modifiers in "fresh" state does not alter the distribution or the relative intensities of the features shown, indicating that structure and morphology of the titania support are not affected.

The spectra of the aged TiO_2 support exhibit a relative increase of the 630−635 cm^{-1} E_g mode compared to the intensity of 513 and 396 cm^{-1} A_{1g} and B_{1g} modes. The observed relative intensity change is related to an intrinsic morphological transition, as observed in our earlier study,[17] correlating the Raman modes with the surface facets of TiO_2. With reference to Mukherjee and Mergel[36] and Taudul et al.,[37] the modes at 396 and 513 cm^{-1} are associated with vibrations of bonds aligned with the *c*-axis, whereas the mode at 635 cm^{-1} is related to vibrations of bonds on the *a*−*b* plane. In situ DRIFTS spectra of the TiO_2 support before and after aging

https://doi.org/10.1021/acs.jpcc.5c08604
J. Phys. Chem. C 2026, 130, 4096−4108

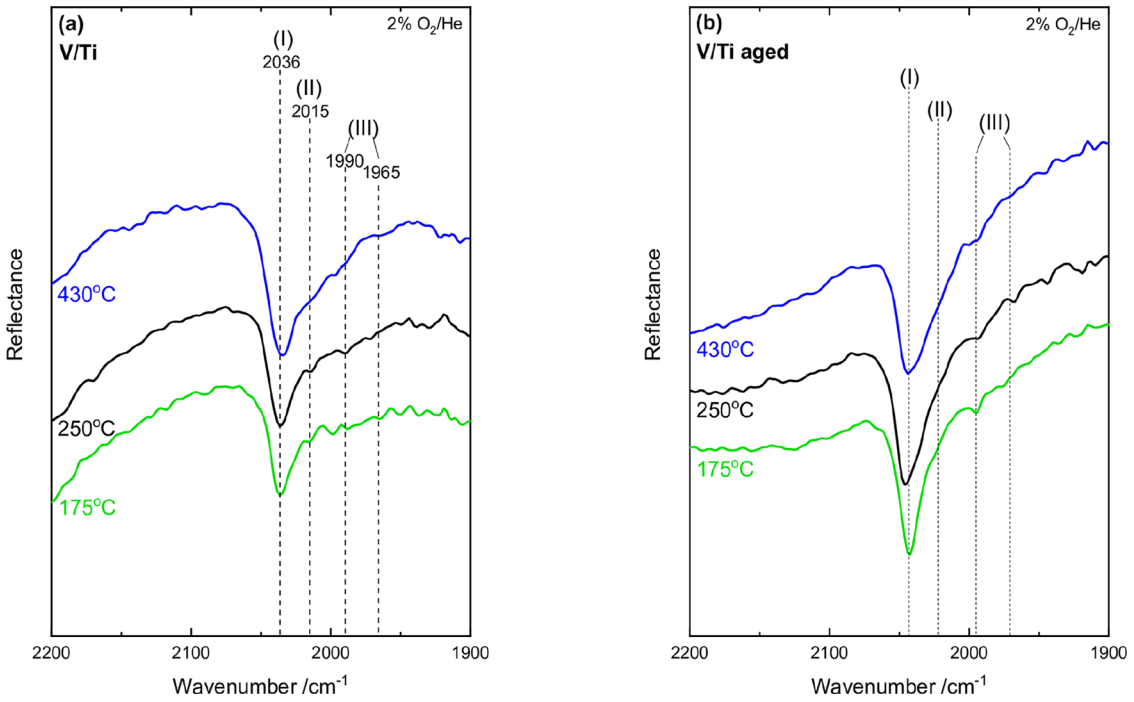

Figure 4. Sequential (430 → 250 → 175 °C) in situ FTIR spectra obtained for unmodified VO_x/TiO_2 before (a) and after (b) the aging procedure under flowing 2% O_2/He at temperatures, as indicated by each spectrum. Resolution, 4 cm^{-1}.

suggest a loss of (100) and (001) facets, while favoring the growth of (101) facets.[17] Hence, the higher relative intensity of the mode at 635 cm^{-1} observed after aging relates to a higher fraction of bonds along the *a*−*b* plane and thus a higher presence of (101) facets. Consequently, the modes at 396 and 513 cm^{-1}, with vibrations along the *c*-axis, relate to the (100) and (001) facets. The presence of vanadium (V/Ti) results in a higher relative increase of the 635 cm^{-1} E_g mode, as vanadium has been shown to promote the observed structural change.[17]

The modified catalysts, VCe/Ti, VNb/Ti, and VSb/Ti, like their counterpart V/Ti, exhibit an increase in the relative intensity of the 630−635 cm^{-1} E_g mode after being subjected to the aging protocol, thereby indicating an increased presence of (101) facets relative to the (100) and (001) terminations. Hence, dispersion of either VO_x or VO_x/MO_x (M = Ce, Nb, Sb) on titania results, after aging, in the promotion of a structural/morphological change of the titania anatase substrate compared to the extent of change undergone by bare titania anatase.

Effect of Temperature and Thermal Aging on Dispersed Vanadium Oxide Structures

To study the temperature dependence and impact of thermal aging on the speciation and structural properties of the dispersed vanadia phase, focused attention was directed to the V═O stretching vibrational properties in the 900−1050 cm^{-1} region. Figure 3 shows the temperature dependence of the in situ Raman spectra obtained for the V/Ti sample in the fresh state (left panels) and after the aging procedure (right panels). The spectra shown in each panel are recorded at a sequence of decreasing temperatures, following the protocol described in the Materials and Methods section. The corresponding in situ Raman spectrum obtained for the bare TiO_2 support (DT51-D) at each temperature is also shown as a separate background in each spectrum. The constituents of the VO_x phase dispersed on titania are well-known and described thoroughly in a recent in situ molecular spectroscopic (Raman, IR) study.[12] At 430 °C, the main Raman band feature shown in the V═O stretching region is asymmetric, consisting of two major components: a majority species with a signature feature at 1024−1026 cm^{-1} assigned to a tetrahedral-like mono-oxo Species-I; a minority species with a characteristic feature at ∼1014−1016 cm^{-1} assigned to a distorted octahedral-like Species-II and a third broader band of lower intensity at the low-wavenumber wing (∼975−1000 cm^{-1}) of the convoluted band envelope. The 975−1000 cm^{-1} band also occurs in the V═O terminal stretching region and, after subtracting the TiO_2 background, appears to comprise at least two components (see e.g., Figure 3c,d). The presence of the three species is also confirmed by the in situ FTIR spectra shown in Figure 4, recorded in the overtone region (2200−1900 cm^{-1}), thereby providing a separation of the overtone counterparts due to the approximate doubling of the distance between the features assigned to each particular species.

The reversible temperature-dependent structural transformations of the dispersed VO_x sites on titania are known from a recent in situ Raman and FTIR spectroscopic investigation and were attributed to surface hydroxylation that takes place by means of a hydrolysis mechanism mediated by water molecules retained by the surface[12]; such water molecules get activated with decreasing temperature.[12] Experimental and theoretical (MD and DFT) studies have shown that water molecules hydrolyze V−O−Ti bonds through dissociative adsorption.[13−15] In addition, low coverages (≤0.8 V nm^{-2}) energetically favor the hydroxyl formation on the titania surface.[10] Figures 3 and 4 show that with decreasing temperature surface hydroxylation occurs. First, by lowering the temperature from 430 to 250 °C, the intensity of feature (I) increases at the expense of the intensity of feature (II) and, second, by further lowering of the temperature, the feature (III) doublet slightly gains intensity relative to feature

https://doi.org/10.1021/acs.jpcc.5c08604
J. Phys. Chem. C 2026, 130, 4096−4108

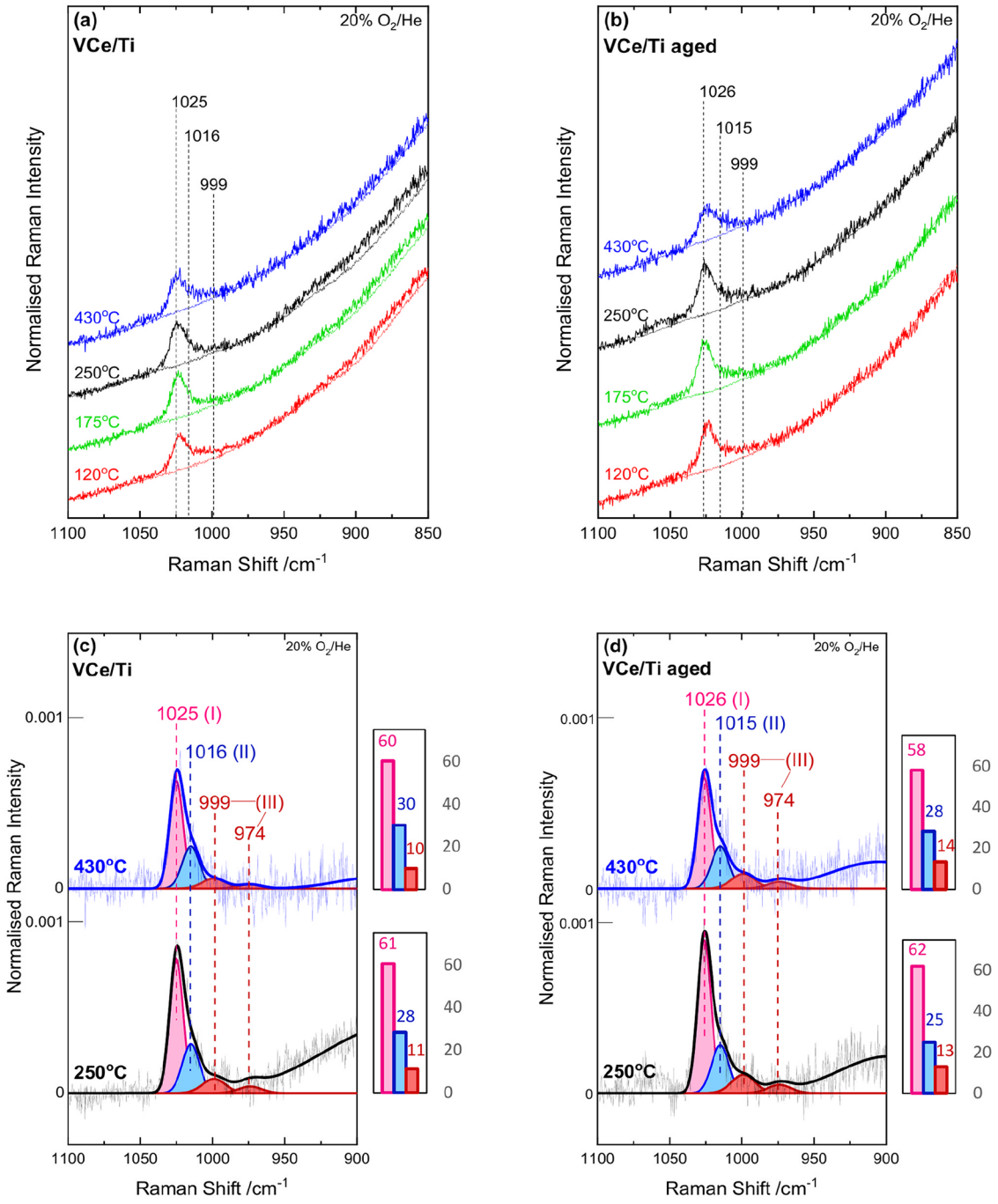

Figure 5. Sequential (430 → 250 → 175 → 120 °C) in situ Raman spectra obtained for CeO_x-modified VO_x/TiO_2 before (a) and after (b) the aging procedure under flowing 20% O_2/He at temperatures, as indicated by each spectrum. The spectra obtained for bare TiO_2 (DT51-D) are also shown as reference background under each spectrum. Peak analysis of in situ Raman spectra of VCe/Ti before (c) and after (d) aging after subtraction of the corresponding TiO_2 (DT51-D) backgrounds at 430 and 250 °C. Recording parameters: see Figure 2 caption.

(I) under in situ conditions. With decreased temperature, water molecules are activated toward hydrolysis of V−O−Ti bonds of Species-II, resulting in the formation of Species-I and two surface hydroxyls.[12] Hence, feature (II) is attenuated, and feature (I) gains intensity and appears sharper. Upon cooling to lower temperatures into the 250−175 °C range, feature (III) gains intensity in relation to the feature (I) and (II) intensity, which is due to the hydrolysis of Species-I, resulting in the formation of Species-III and two surface hydroxyls.[12] It should be noted that the observed structural changes are reversible.

The in situ Raman spectra recorded after the aging procedure, where each sample was treated at 580 °C for 100 h, indicate a structural transformation of the dispersed VO_x species. In the spectrum obtained at 430 °C, a broad feature around 900−950 cm^{-1} is discerned, which by further temperature lowering progressively gains intensity at the expense of the features of Species-I and Species-II. The growth of a broad feature around 900−950 cm^{-1} with increasing coverage has been related to the increase of the polymeric VO_x site population and assigned to V−O−V or O−V−O modes.[6,38−40] The results of the presented spectra are in

https://doi.org/10.1021/acs.jpcc.5c08604
J. Phys. Chem. C 2026, 130, 4096−4108

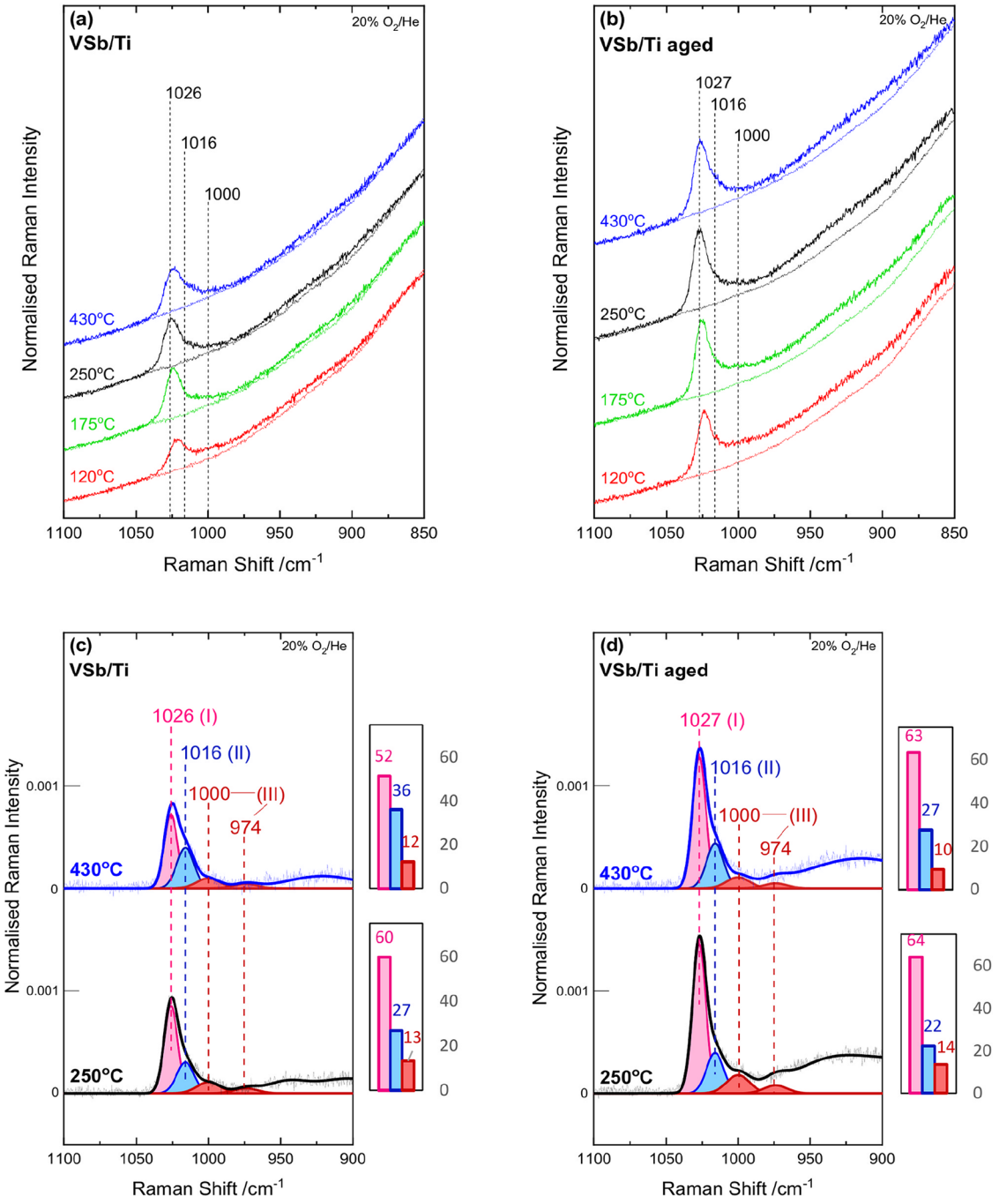

Figure 6. Sequential (430 → 250 → 175 → 120 °C) in situ Raman spectra obtained for SbO_x-modified VO_x/TiO_2 before (a) and after (b) the aging procedure under flowing 20% O_2/He at temperatures, as indicated by each spectrum. The spectra obtained for bare TiO_2 (DT51-D) as also shown as reference background under each spectrum. Peak analysis of in situ Raman spectra of VSb/Ti before (c) and after (d) aging after subtraction of the corresponding TiO_2 (DT51-D) backgrounds at 430 and 250 °C. Recording parameters: see Figure 2 caption.

full alignment with the previewed existence of distinct monomeric species for the low-coverage 0.4 V nm^{-2} nonaged sample,[12] more specifically, with a majority mono-oxo monomeric tetrahedral-like Species-I with tetracoordinated vanadium (CN_V = 4) and a minority octahedral-like Species-II with pentacoordinated vanadium (CN_V = 5). The spectra after the aging procedure suggest the agglomeration of the dispersed VO_x species through the formation of V−O−V linkages. Importantly, lowering of the SSA upon aging results in an increase of the V surface density from 0.4 to 1.4 V nm^{-2}, thereby accounting for the association of isolated VO_x units toward polymeric $(VO_x)_n$ domains and an increase of the normalized Raman intensities of, e.g., Species-I and Species-II in the aged sample relative to its nonaged counterpart. Surface diffusion and mobility of dispersed species induced by heating the sample at 580 °C for 100 h facilitate the association of dispersed VO_x units in the resulting environment of reduced SSA.

Based on a procedure previously described,[12] a peak analysis procedure was undertaken in the V−O terminal stretching region to identify the separate contributions to the pertinent band envelope and to corroborate the proposals for the

https://doi.org/10.1021/acs.jpcc.5c08604
J. Phys. Chem. C 2026, 130, 4096−4108

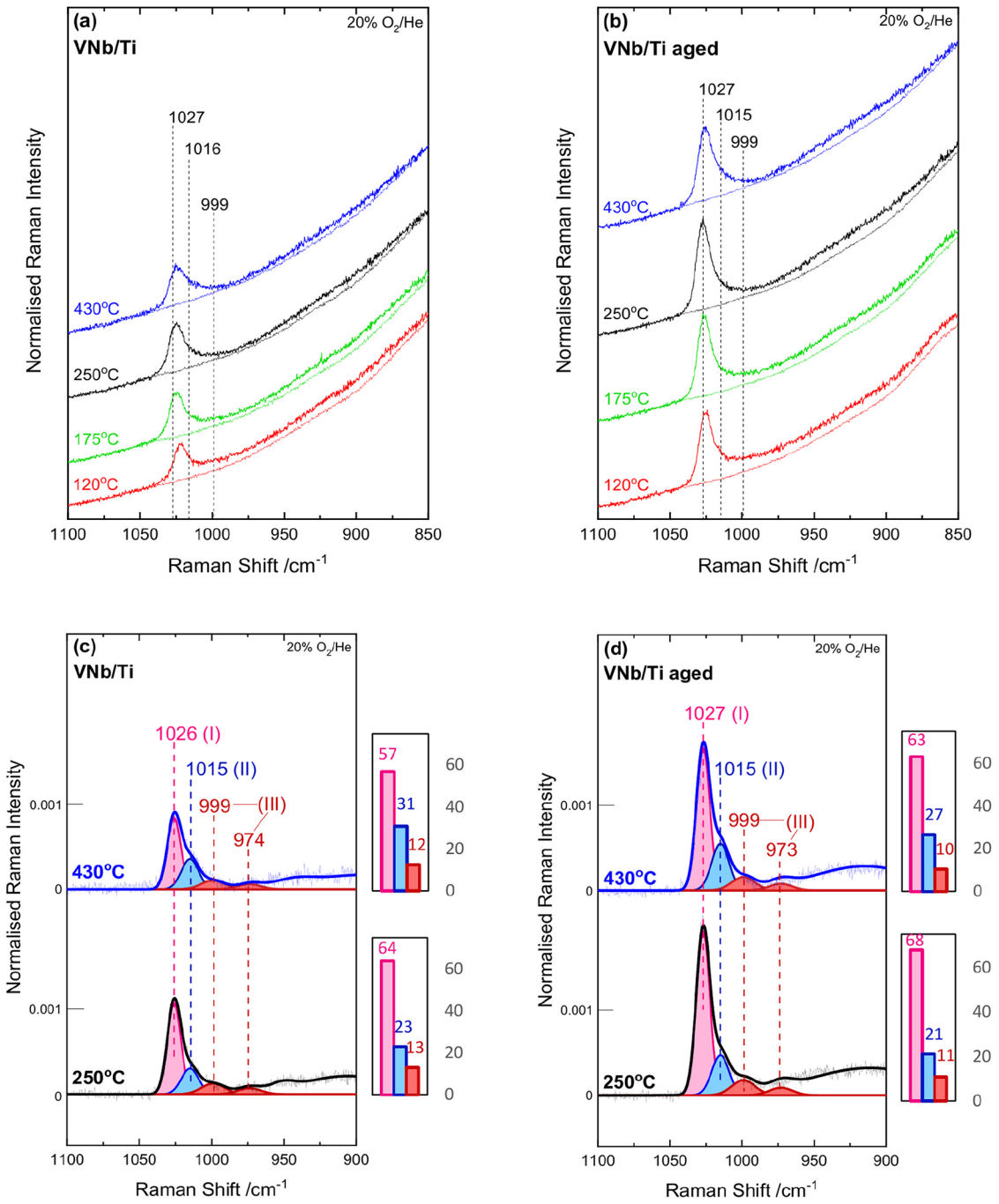

Figure 7. Sequential in situ Raman spectra obtained for NbO_x-modified VO_x/TiO_2 before (a) and after (b) the aging procedure under flowing 20% O_2/He at temperatures, as indicated by each spectrum. The spectra obtained for bare TiO_2 (DT51-D) are also shown as reference background under each spectrum. Peak analysis of in situ Raman spectra of VNb/Ti before (c) and after (d) aging after subtraction of the corresponding TiO_2 (DT51-D) backgrounds at 430 and 250 °C. Recording parameters: see Figure 2 caption.

occurrence of distinct VO_x sites. Before undertaking the peak fitting procedure, the spectrum of the pure support (DT51-D) recorded at each temperature was subtracted from the spectrum obtained for each sample. The peak analysis is confined to the spectra recorded at 430 and 250 °C for two reasons. First, due to the relevance of the two above temperatures for the NH_3−SCR process[28] and, second, due to the distortive impact of the V−O−V features at lower temperatures. Bands (I), (II), and (III) occur in the terminal V═O stretching region and hence originate from V═O sites existing in distinct coordination environments or belonging to polyoxo (e.g., dioxo) configurations. Oxo-metallic sites with mono-oxo termination configuration possess one single M═O stretching mode, while a site with dioxo $M(=O)_2$ termination configuration possesses a pair of terminal stretching modes, i.e., a symmetric ν_s mode and an antisymmetric ν_{as} mode, of which the ν_s mode has a higher Raman intensity than its counterpart ν_{as} mode and their mutual separation complies with $\nu_s-\nu_{as} \sim 10-40$ cm^{-1} depending on the O═M═O angle.[30,41] Bands (I) and (II) have already been assigned to distinct mono-oxo species because by lowering the temperature from 430 to 250 °C, the intensity of band (I) increases at the expense of band

https://doi.org/10.1021/acs.jpcc.5c08604
J. Phys. Chem. C 2026, 130, 4096−4108

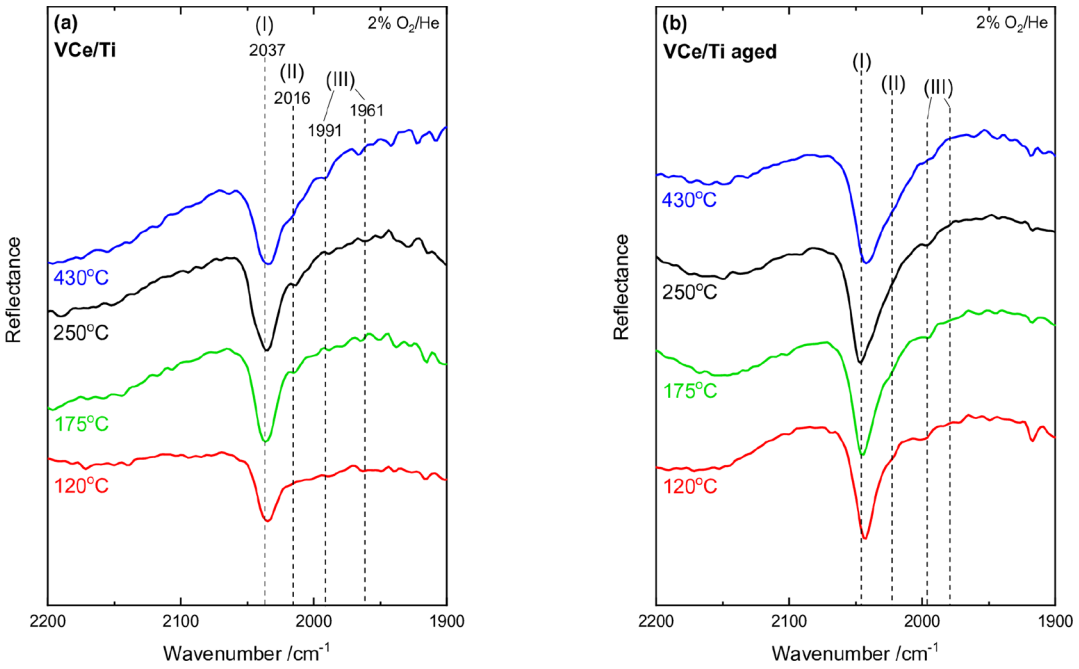

Figure 8. Sequential (430 → 250 → 175 °C) in situ FTIR spectra obtained for CeO_x-modified VO_x/TiO_2 before (a) and after (b) the aging procedure under flowing 2% O_2/He at temperatures, as indicated by each spectrum. Resolution, 4 cm^{-1}.

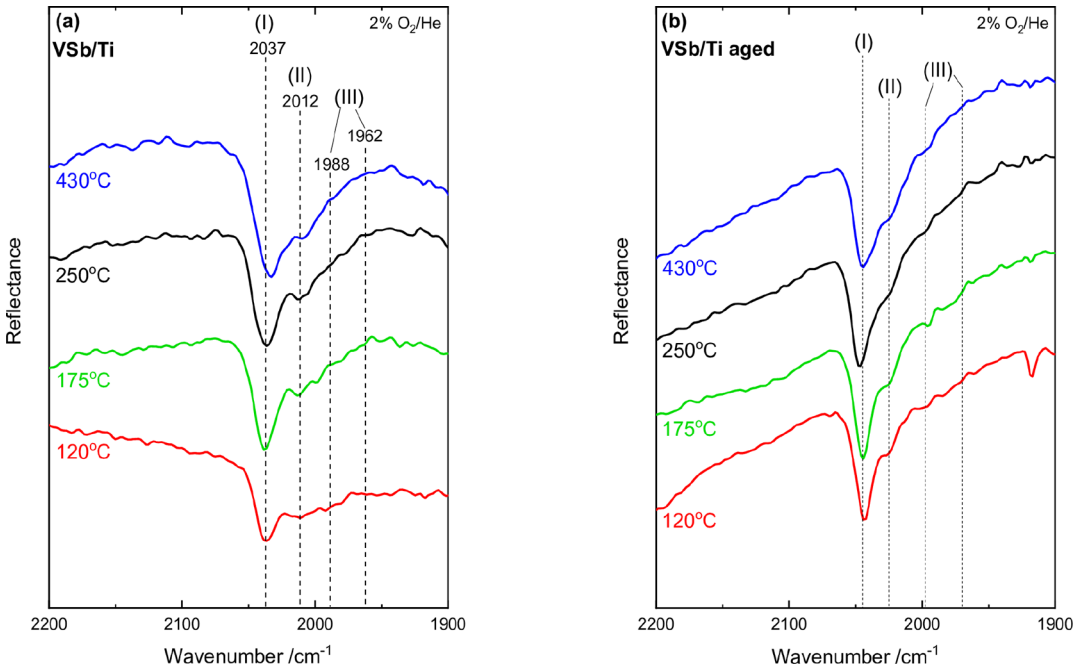

Figure 9. Sequential (430 → 250 → 175 °C) in situ FTIR spectra obtained for SbO_x-modified VO_x/TiO_2 before (a) and after (b) the aging procedure under flowing 2% O_2/He at temperatures, as indicated by each spectrum. Resolution, 4 cm^{-1}.

(II). Whereas the vibrational stretching wavenumbers of terminal mono-oxo V═O site are expected in the ∼1015−1030 cm^{-1} region,[1,2,5,7,12,41,42] the corresponding wavenumbers for dioxo $V(═O)_2$ sites occur near and below 1000 cm^{-1}.[41,43] Hence, if the broad feature observed at ∼975−1000 cm^{-1} originates from a dioxo $V(═O)_2$ site, it should conform to the following conditions: (i) comprise two components; (ii) the high-wavenumber component (ν_s) should be stronger than its low-wavenumber counterpart (ν_{as}); (iii) $\nu_s-\nu_{as}$ ∼ 10−40 cm^{-1}; and (iv) the ν_s/ν_{as} intensity ratio should be independent of temperature. The principles and criteria used for the peak analysis include the following: (1) the occurrence of four bands originating from three species, based on the evidence from the combined in situ Raman/FTIR spectra as follows; (i) one band, occurring at the highest wavenumber due to V═O stretching of Species-I; (ii) one band, at the second highest wavenumber due to V═O stretching of Species-II; and (iii) two bands due to the ν_s/ν_{as} pair assigned to Species-III with $\nu_s-\nu_{as}$ ∼ 10−40 cm^{-1}. (2) A fixed width and position for each band (allowing for the ±1 cm^{-1} precision for each measurement) for each studied sample at each temperature. (3) Fixed relative I_s/I_{as} intensities for the dioxo Species-III with

https://doi.org/10.1021/acs.jpcc.5c08604
J. Phys. Chem. C 2026, 130, 4096−4108

allowance for larger widths for the dioxo $\nu(=O)_2$ stretches compared to their mono-oxo $\nu(V=O)$ counterparts.

The results of the peak analysis shown in Figure 3 confirm the previously reached conclusions[12] and provide further insight pertaining to the effect of thermal aging on the speciation of the dispersed VO_x phase. Hence, by lowering the temperature, the extent of Species-I presence is increased at the expense of Species-II, for both fresh and aged samples due to the previously proposed Species-II to Species-I transformation.[12] Additionally, as indicated by comparing the peak analysis results for the fresh and aged samples at the same temperature, thermal aging strengthens the prevalence of Species-I over Species-II. Previously, it has been proposed that the occurrence of mono-oxo tetracoordinated VO_4 units (Species-I) is favored on anatase (101) facets, while Species-II (mono-oxo octahedral-like penta-coordinated VO_5 units) occur on anatase (001) facets.[10,12] The relative increase of (101) anatase terminations resulting from thermal aging (see previous section) accounts for the relative increase of Species-I over Species-II in the aged sample.

Effect of Modifiers and Thermal Aging on Dispersed Vanadium Oxide Species

Figures 5−7 show the temperature dependence of the in situ Raman spectra in the wavenumber range pertaining to the V=O terminal stretching modes as well as to the V−O−V and O−V−O modes (1050−850 cm^{-1}), obtained for the modified VCe/Ti, VSb/Ti, and VNb/Ti catalyst samples in the temperature range of 430−120 °C, respectively. The spectra shown in each panel are recorded at a sequence of decreasing temperatures (430−120 °C). The top panels in each figure portray the normalized in situ Raman spectra for each sample together with the respective in situ Raman spectra of the bare titania support (adapted background trace under each spectrum) at temperatures indicated by each spectrum. The left panels in each case pertain to the fresh calcined samples, and the right panels pertain to samples subjected to thermal aging at 580 °C for 100 h. The bottom panels show the corresponding results of the peak analysis procedure that was undertaken after subtracting the spectrum of the titania support from the spectrum obtained for each sample. Figures 8 and 9 show the corresponding temperature-dependent in situ FTIR spectra obtained for the modified VCe/Ti and VSb/Ti samples, and Figure S1 shows the in situ FTIR spectra obtained for the VNb/Ti catalysts. Again, the left panels in each case show spectra obtained for fresh calcined samples, while the right panels show spectra obtained for samples subjected to thermal aging. The effects of the modification with either cerium (Ce), niobium (Nb), and antimony (Sb) oxide on VO_x species distribution and structural transformation stability were investigated and compared with the unmodified V/Ti as reference.

The Raman spectra of the fresh calcined Ce-modified sample Ce/Ti, depicted in Figure 5, show an increased normalized intensity for the Species-I band at 1025 cm^{-1}, compared to the unmodified V/Ti reference. The peak analysis reveals that Species-I is the prevailing species in the VCe/Ti sample, with an extent of presence that exceeds the one in the unmodified reference, namely, the Species-I/Species-II ratio is raised from 1.4 to 2.0 upon modification with Ce. Invariably, upon cooling to 250 °C, the Species-II to Species-I transformation[12] takes place. After thermal aging, a comparison of the peak analysis results shows a limited increase in Species-I over Species-II. Moreover, limited features corresponding to the characteristic of V−O−V and/or O−V−O bridging modes around 850−950 cm^{-1} were observed, which are accounted for by the limited lowering of the SSA upon thermal aging (from 83 to 53 m^2 g^{-1}) that results in a moderate increase from 0.5 to 0.8 V nm^{-2} in vanadium surface density. Overall, the changes induced upon thermal aging of the VCe/Ti sample are accounted mainly by the moderate lowering of the SSA, which results in a slight increase of the V surface density. Hence, whereas modification of the V/Ti with Ce results in an increased presence of Species-I relative to Species-II, thermal aging of the VCe/Ti sample does not significantly perturb the speciation of the dispersed vanadia phase. The in situ FTIR spectra shown in Figure 8 corroborate the observations above, namely, providing a visible separation of V=O stretching modes due to Species-I and Species-II (due to the approximate doubling of their mutual distance in the overtone region) and a slight increase of the Species-I/Species-II ratio upon aging.

The in situ Raman spectra obtained for the fresh calcined samples of catalysts modified with either antimony or niobium (VSb/Ti and VNb/Ti), shown in the left panels of Figures 6 and 7, exhibit a higher band intensity for the prevailing Species-I at 1026 cm^{-1} compared to the counterpart fresh calcined unmodified V/Ti sample. The same trend is followed, as shown by the peak analysis results, for the band intensity due to Species-II and Species-III. Additionally, due to the significant increase in surface density upon aging (by about 1 V nm^{-2}), the dispersed oxo-metallic faces for the aged VSb/Ti and VNb/Ti samples exhibit a substantial increase in the extent of association compared to the corresponding fresh samples, as evidenced from the peak analysis results (Figures 6 and 7) in the 850−950 cm^{-1} region. Broad bands in this region have previously been assigned to either V−O−V or O−V−O modes as well as to V−O−Sb and V−O−Nb bridging modes.[12,44−47] Additionally, as expected, lowering the temperature from 430 to 250 °C results in a transformation of Species-II into Species-I. Notably, the increase in the normalized band intensities due to the distinct species formed by Sb or Nb modification does not necessarily imply a commensurate increase in the respective populations. In contrast, it can be due to alterations in the mechanisms that give rise to the band intensity, namely, the so-called intensity selection rules.

The in situ Raman spectra obtained for the thermally aged samples (shown in the right panels of Figures 6 and 7) show a large increase of the Species-I/Species-II ratio for both VSb/Ti and VNb/Ti samples. Thermal aging, apart from a lowering of the SSA and a concomitant increase in V surface density (Table 1), results in a structural/morphological transformation of the anatase support, thereby resulting in a higher presence of (101) facet terminations that are known to favor the occurrence of trianchored mono-oxo tetracoordinated VO_4 sites, while a lower presence of (001) facets leads to a lower occurrence of the tetra-anchored penta-coordinated VO_5 sites.[10,12] Moreover, thermal aging results in an increase of the extent of associated domains' presence, evidenced by the higher intensities of the broad features in the 900−975 cm^{-1} range in the spectra obtained for the aged samples (right panels, Figures 6 and 7). Additionally, lowering the temperature from 430 to 250 °C invariably results in the previously established Species-I to Species-II transformation.[12] The in situ FTIR spectra, shown for example in Figure 9 for the Sb-modified sample corroborate the above findings, namely: (i)

https://doi.org/10.1021/acs.jpcc.5c08604
J. Phys. Chem. C 2026, 130, 4096−4108

the occurrence of distinct VO_x species; (ii) the Species-II to Species-I transformation when lowering the temperature from 430 to 250 °C; and (iii) the prevalence of Species-I over Species-II at 430 and 250 °C as a consequence of thermal aging.

Implications for Catalysis

Elucidating the speciation of dispersed VO_x sites with distinct configurations can provide valuable information about the relationship between molecular structure and reactivity for the catalyst formulations studied. Notably, determining the identity of active sites is a formidable challenge, given the eventual complexity of the active phase that can itself be heterogeneous. Additionally, the majority of species among the distinct VO_x configurations constituting the dispersed phase are not necessarily the active ones. To date, the heterogeneity of the deposited transition metal oxide phase has often been addressed in the catalysis literature.[12,30,48−55] Hence, exploring the conditions allowing for selective tuning of the configuration of the dispersed oxo-metallic sites may be of value to achieve improved catalyst activity. The effects of coverage and reversible temperature-dependent transformations have been thoroughly addressed in several cases.[12,30,53−55]

The present work expands the exploration of conditions for tuning the configurations of dispersed VO_x sites on titania-(anatase) by examining the effects of: (a) catalyst phase modification with the inclusion of CeO_x, NbO_x, and SbO_x modifiers at an M/V = 1 (M = Ce, Nb, Sb) on the configurational characteristics of dispersed VO_x species and (b) thermal aging at 580 °C for 100 h. Both parameters are found to affect the speciation of the dispersed heterogeneous VO_x phase, in both cases in favor of increasing the ratio of the Species-I/Species-II presence. The effect is governed for both cases by means of a mechanism based on selective preference of species anchoring in anatase facets.

The exploration of the catalyst phase modification and thermal aging on the VO_x configurational characteristics is here restricted to low-loaded VO_x/TiO_2(anatase) catalysts. As such, they are not made for practical catalysis but rather designed to ensure that the extent of VO_x species occurs in isolated form, thereby allowing the study of their vibrational properties by limiting eventual effects of vibrational coupling, hence resulting in as clear as possible spectroscopic signatures for the distinct configurations present. Therefore, although the new insight is not readily generalizable to catalysts with high coverage, e.g., monolayer coverage, the results expand the understanding of the catalyst-supported phase behavior at the molecular level, with an aim to help its correlations with reactivity and catalytic performance.

CONCLUSIONS

Modification of V/Ti catalysts with either Ce, Sb, or Nb preserves the established occurrence of three distinct species within the dispersed VO_x phase in low coverage catalysts. Species-I with a trianchored mono-oxo tetracoordinated VO_4 configuration prevails at temperatures of 175−430 °C in all samples, followed by Species-II with a tetra-anchored mono-oxo pentacoordinated VO_5 configuration and a minority Species-III with a dioxo termination configuration. To conclude, lowering the temperature from 430 to 250 °C results in a transformation of Species-II into Species-I. This transformation is mediated by surface-retained water molecules that are activated at the lower temperature. Upon further lowering of the temperature to 175 and then 120 °C, Species-I transforms into Species-III. Modification of V/Ti catalysts with either Ce, Sb, or Nb results (to different extents) in an increase of the Species-I/Species-II ratio, indicating a possible preference of CeO_x, SbO_x, and NbO_x sites to exist on (001) facets. Thermal aging at 580 °C for 100 h results in structural/morphological transformations of the titania anatase support, resulting in a higher abundance of (101) facets, thereby favoring an increased occurrence of Species-I. Thermal aging also results in a higher extent of association/polymerization of V surface oxides through formation of V−O−V and/or V−O−M (M = Ce, Sb, Nb) linkages, mainly due to the increased V and M (M = Ce, Sb, Nb) surface densities caused by lower SSA.

ASSOCIATED CONTENT

Supporting Information

The Supporting Information is available free of charge at https://pubs.acs.org/doi/10.1021/acs.jpcc.5c08604.

In situ FTIR spectra of the VNb/Ti catalyst in 2% O_2 at 120, 175, 250, and 430 °C before and after aging (PDF)

AUTHOR INFORMATION

Corresponding Authors

Per-Anders Carlsson − *Department of Chemistry and Chemical Engineering and Competence Centre for Catalysis, Chalmers University of Technology, Gothenburg 412 58, Sweden;* orcid.org/0000-0001-6318-7966; Email: per-anders.carlsson@chalmers.se

Soghomon Boghosian − *Department of Chemical Engineering, University of Patras, Patras 26504, Greece; Institute of Chemical Engineering Sciences, FORTH/ICE-HT, Patras 26504, Greece*; Email: bogosian@chemeng.upatras.gr

Authors

Alexander Nellessen − *Department of Chemistry and Chemical Engineering and Competence Centre for Catalysis, Chalmers University of Technology, Gothenburg 412 58, Sweden;* orcid.org/0000-0002-6532-4212

Iliana-Maria Stergiou − *Department of Chemical Engineering, University of Patras, Patras 26504, Greece;* orcid.org/0009-0002-3142-022X

Theocharis Kentri − *Department of Chemical Engineering, University of Patras, Patras 26504, Greece*

Roberta Villamaina − *Johnson Matthey Technology Centre, Reading RG4 9NH, U.K.*

Anna Martinelli − *Department of Chemistry and Chemical Engineering, Chalmers University of Technology, Gothenburg 412 58, Sweden;* orcid.org/0000-0001-9885-5901

Andreas Schaefer − *Department of Chemistry and Chemical Engineering and Competence Centre for Catalysis, Chalmers University of Technology, Gothenburg 412 58, Sweden;* orcid.org/0000-0001-6578-5046

Complete contact information is available at: https://pubs.acs.org/10.1021/acs.jpcc.5c08604

Notes

The authors declare no competing financial interest.

https://doi.org/10.1021/acs.jpcc.5c08604
J. Phys. Chem. C 2026, 130, 4096−4108

■ ACKNOWLEDGMENTS

This work was financially supported by the Swedish Energy Agency through the FFI program "Ultraefficient recyclable De-NO_x catalysts for biofuel and hybrid powertrains" (no. 51318-1) and by the Competence Centre for Catalysis, which is hosted by Chalmers University of Technology and financially supported by the Swedish Energy Agency and the member companies AB Volvo, ECAPS AB, Johnson Matthey Plc, Perstorp AB, Preem AB, Scania CV AB, and Umicore AG & Co. KG.

■ REFERENCES

(1) Dunn, J. P.; Stenger, H. G., Jr; Wachs, I. E. Oxidation of sulfur dioxide over supported vanadia catalysts: molecular structure−reactivity relationships and reaction kinetics. *Catal. Today* **1999**, *51*, 301−318.

(2) Christodoulakis, A.; Machli, M.; Lemonidou, A. A.; Boghosian, S. Molecular structure and reactivity of vanadia-based catalysts for propane oxidative dehydrogenation studied by in situ Raman spectroscopy and catalytic activity measurements. *J. Catal.* **2004**, *222*, 293−306.

(3) Mamedov, E.; Corberán, V. C. Oxidative dehydrogenation of lower alkanes on vanadium oxide-based catalysts. The present state of the art and outlooks. *Appl. Catal., A* **1995**, *127*, 1−40.

(4) Pârvulescu, V. I.; Grange, P.; Delmon, B. Catalytic removal of NO. *Catal. Today* **1998**, *46*, 233−316.

(5) Weckhuysen, B. M.; Keller, D. E. Chemistry, spectroscopy and the role of supported vanadium oxides in heterogeneous catalysis. *Catal. Today* **2003**, *78*, 25−46.

(6) Vuurman, M. A.; Wachs, I. E.; Hirt, A. M. Structural determination of supported V_2O_5-WO_3/TiO_2 catalysts by in situ Raman spectroscopy and X-ray photoelectron spectroscopy. *J. Phys. Chem.* **1991**, *95*, 9928−9931.

(7) Strunk, J.; Bañares, M. A.; Wachs, I. E. Vibrational spectroscopy of oxide overlayers. *Top. Catal.* **2017**, *60*, 1577−1617.

(8) Ek, M.; Arnarson, L.; Moses, P. G.; Rasmussen, S. B.; Skoglundh, M.; Olsson, E.; Helveg, S. Probing surface-sensitive redox properties of VO_x/TiO_2 catalyst nanoparticles. *Nanoscale* **2021**, *13*, 7266−7272.

(9) Du, Y.-J.; Li, Z. H.; Fan, K.-N. Periodic density functional theory studies of the VO_x/TiO_2 (anatase) catalysts: Structure and stability of monomeric species. *Surf. Sci.* **2012**, *606*, 956−964.

(10) Arnarson, L.; Rasmussen, S. B.; Falsig, H.; Lauritsen, J. V.; Moses, P. G. Coexistence of square pyramidal structures of oxo vanadium (+5) and (+4) species over low-coverage VO_x/TiO_2 (101) and (001) anatase catalysts. *J. Phys. Chem. C* **2015**, *119*, 23445−23452.

(11) Guerrero-Pérez, M. O.; Martínez-Huerta, M. V.; Bañares, M. A. *Molecularly dispersed vanadium oxide: structure−reactivity relationships for reducibility and hydrocarbon oxidation*; RSC: 2020.

(12) Kentri, T.; Tsevis, A.; Boghosian, S. Heterogeneity of the vanadia phase dispersed on titania. Co-existence of distinct mono-oxo VO_x sites. *Dalton Transactions* **2023**, *52*, 7495−7511.

(13) Lewandowska, A. E.; Calatayud, M.; Tielens, F.; Banares, M. A. Dynamics of hydration in vanadia−titania catalysts at low loading: a theoretical and experimental study. *J. Phys. Chem. C* **2011**, *115*, 24133−24142.

(14) Lewandowska, A. E.; Calatayud, M.; Tielens, F.; Banares, M. A. Hydration dynamics for vanadia/titania catalysts at high loading: a combined theoretical and experimental study. *J. Phys. Chem. C* **2013**, *117*, 25535−25544.

(15) Rasmussen, S. B.; Portela, R.; Bazin, P.; Ávila, P.; Bañares, M. A.; Daturi, M. Transient operando study on the NH_3/NH_4^+ interplay in V-SCR monolithic catalysts. *Applied Catalysis B: Environmental* **2018**, *224*, 109−115.

(16) Won, J. M.; Kim, M. S.; Hong, S. C. The cause of deactivation of VO_x/TiO_2 catalyst by thermal effect and the role of tungsten addition. *Chem. Eng. Sci.* **2021**, *229*, No. 116068.

(17) Nellessen, A.; Schaefer, A.; Martinelli, A.; Raj, A.; Newman, A.; Carlsson, P.-A. Impact of vanadium loading and thermal aging on the surface properties of titania-supported vanadium oxide. *J. Phys. Chem. C* **2024**, *128*, 2894−2908.

(18) Oliverl, G.; Ramis, G.; Busca, G.; Sanchez Escribanob, V. Thermal stability of vanadia-titania catalysts. *J. Mater. Chem.* **1993**, *3*, 1239−1249.

(19) Jeong, Y. E.; Kumar, P. A.; Ha, H. P.; Lee, K.-y. Highly active Sb−V−CeO_2/TiO_2 catalyst under low sulfur for NH_3-SCR at low temperature. *Catal. Lett.* **2017**, *147*, 428−441.

(20) Jeong, Y. E.; Kumar, P. A.; Huong, D. T.; Ha, H. P.; Lee, K.-Y. In situ-DRIFTS study of Sb−V−CeO_2/TiO_2 catalyst under standard and fast NH_3-SCR conditions. *Top. Catal.* **2017**, *60*, 755−762.

(21) Jeong, Y. E.; Kumar, P. A.; Ha, H. P.; Lee, K.-y. Effect of hydrothermal aging on NO_x reduction performance for Sb−V−CeO_2/TiO_2 catalyst. *Res. Chem. Intermed.* **2018**, *44*, 6803−6829.

(22) Kumar, P. A.; Jeong, Y. E.; Ha, H. P. Low temperature NH_3-SCR activity enhancement of antimony promoted vanadia-ceria catalyst. *Catal. Today* **2017**, *293*, 61−72.

(23) Du, X.; Gao, X.; Fu, Y.; Gao, F.; Luo, Z.; Cen, K. The co-effect of Sb and Nb on the SCR performance of the V_2O_5/TiO_2 catalyst. *J. Colloid Interface Sci.* **2012**, *368*, 406−412.

(24) Lian, Z.; Liu, F.; He, H.; Liu, K. Nb-doped VO_x/CeO_2 catalyst for NH_3-SCR of NO_x at low temperatures. *RSC Adv.* **2015**, *5*, 37675−37681.

(25) Lian, Z.; Liu, F.; Shan, W.; He, H. Improvement of Nb doping on SO_2 resistance of VO_x/CeO_2 catalyst for the selective catalytic reduction of NO_x with NH_3. *J. Phys. Chem. C* **2017**, *121*, 7803−7809.

(26) Bae, Y. K.; Kim, T.-W.; Kim, J.-R.; Kim, Y.; Ha, K.-S.; Chae, H.-J. Enhanced SO_2 tolerance of V_2O_5-Sb_2O_3/TiO_2 catalyst for NO reduction with co-use of ammonia and liquid ammonium nitrate. *Journal of Industrial and Engineering Chemistry* **2021**, *96*, 277−283.

(27) Kwon, D. W.; Kim, D. H.; Hong, S. C. Promotional effect of antimony on the selective catalytic reduction NO with NH_3 over V-Sb/Ti catalyst. *Environmental Technology* **2019**, *40*, 2577−2587.

(28) Nellessen, A.; Villamaina, R.; Schaefer, A.; Raj, A.; Newman, A.; Martinelli, A.; Carlsson, P.-A. Antimony modification of VO_x/TiO_2 NH_3-SCR catalysts and the effect of thermal aging. *J. Catal.* **2025**, *450*, No. 116303.

(29) Tsilomelekis, G.; Boghosian, S. On the configuration, molecular structure and vibrational properties of MoO_x sites on alumina, zirconia, titania and silica. *Catalysis Science & Technology* **2013**, *3*, 1869−1888.

(30) Andriopoulou, C.; Boghosian, S. Tuning the configuration of dispersed oxometallic sites in supported transition metal oxide catalysts: A temperature dependent Raman study. *Catal. Today* **2019**, *336*, 74−83.

(31) Andriopoulou, C.; Harris, D.; Stephenson, H.; Efstathiou, A. M.; Boghosian, S. In situ Raman spectroscopy as a tool for discerning subtle structural differences between commercial (Ce, Zr) O_2-based OSC materials of identical composition. *Catalysts* **2020**, *10*, 462.

(32) Ohsaka, T.; Izumi, F.; Fujiki, Y. Raman spectrum of anatase, TiO_2. *J. Raman Spectrosc.* **1978**, *7*, 321−324.

(33) Chastain, J.; King, Jr, R. C. *Handbook of X-ray photoelectron spectroscopy*; Perkin-Elmer Corporation: 1992; Vol. *40*, p 25.

(34) Giarola, M.; Sanson, A.; Monti, F.; Mariotto, G.; Bettinelli, M.; Speghini, A.; Salviulo, G. Vibrational dynamics of anatase TiO_2: Polarized Raman spectroscopy and ab initio calculations. *Physical Review B—Condensed Matter and Materials. Physics* **2010**, *81*, No. 174305.

(35) Beattie, I.; Gilson, T. Oxide phonon spectra. *Journal of the Chemical Society A: Inorganic, Physical, Theoretical* **1969**, 2322−2327.

(36) Mukherjee, S.; Mergel, D. Thickness dependence of the growth of magnetron-sputtered TiO_2 films studied by Raman and optical transmittance spectroscopy. *J. Appl. Phys.* **2013**, *114*, No. 013501.

(37) Taudul, B.; Tielens, F.; Calatayud, M. On the origin of raman activity in anatase TiO_2 (nano) materials: an ab initio investigation of surface and size effects. *Nanomaterials* **2023**, *13*, 1856.

https://doi.org/10.1021/acs.jpcc.5c08604
J. Phys. Chem. C 2026, 130, 4096−4108

(38) Wachs, I.; Jehng, J.-M.; Deo, G.; Hu, H.; Arora, N. Redox properties of niobium oxide catalysts. *Catal. Today* **1996**, *28*, 199−205.
(39) Went, G. T.; Leu, L.-J.; Bell, A. T. Quantitative structural analysis of dispersed vanadia species in TiO_2 (anatase)-supported V_2O_5. *J. Catal.* **1992**, *134*, 479−491.
(40) Machej, T.; Haber, J.; Turek, A. M.; Wachs, I. E. Monolayer V_2O_5/TiO_2 and MoO_3/TiO_2 catalysts prepared by different methods. *Appl. Catal.* **1991**, *70*, 115−128.
(41) Nakamoto, K. *Infrared and Raman spectra of inorganic and coordination compounds, Part B: Applications in coordination, organometallic, and bioinorganic chemistry*; John Wiley & Sons: 2009.
(42) Giakoumelou, I.; Fountzoula, C.; Kordulis, C.; Boghosian, S. Molecular structure and catalytic activity of V2O5/TiO2 catalysts for the SCR of NO by NH3: In situ Raman spectra in the presence of O2, NH3, NO, H2, H2O, and SO2. *J. Catal.* **2006**, *239*, 1−12.
(43) Boghosian, S. Vibrational modes and structure of vanadium (V) complexes in M 2 SO 4−V 2 O 5 (M= K or Cs) molten salt mixtures. *Journal of the Chemical Society, Faraday Transactions* **1998**, *94*, 3463−3469.
(44) Pittman, R. M.; Bell, A. T. Raman studies of the structure of niobium oxide/titanium oxide (Nb_2O_5/TiO_2). *J. Phys. Chem.* **1993**, *97*, 12178−12185.
(45) Guerrero-Pérez, M.; Fierro, J.; Banares, M. Effect of synthesis method on stabilized nano-scaled Sb−V−O catalysts for the ammoxidation of propane to acrylonitrile. *Top. Catal.* **2006**, *41*, 43−53.
(46) Guerrero-Pérez, M. O.; Fierro, J.; Bañares, M. A. Niobia-supported Sb−V−O catalysts for propane ammoxidation: effect of catalyst composition on the selectivity to acrylonitrile. *Phys. Chem. Chem. Phys.* **2003**, *5*, 4032−4039.
(47) Golinska-Mazwa, H.; Rojas, E.; López-Medina, R.; Ziolek, M.; Banares, M.; Guerrero-Pérez, M. Niobiosilica Materials as Attractive Supports for Sb−V−O Catalysts. *Top. Catal.* **2012**, *55*, 837−845.
(48) Eibl, S.; Gates, B.; Knözinger, H. Structure of WO_x/TiO_2 catalysts prepared from hydrous titanium oxide hydroxide: influence of preparation parameters. *Langmuir* **2001**, *17*, 107−115.
(49) Weckhuysen, B. M. Determining the active site in a catalytic process: Operando spectroscopy is more than a buzzword. *Phys. Chem. Chem. Phys.* **2003**, *5*, 4351−4360.
(50) Lwin, S.; Wachs, I. E. Olefin metathesis by supported metal oxide catalysts. *ACS Catal.* **2014**, *4*, 2505−2520.
(51) Lwin, S.; Keturakis, C.; Handzlik, J.; Sautet, P.; Li, Y.; Frenkel, A. I.; Wachs, I. E. Surface ReO_x Sites on Al_2O_3 and their molecular structure−reactivity relationships for olefin metathesis. *ACS Catal.* **2015**, *5*, 1432−1444.
(52) Ding, K.; Gulec, A.; Johnson, A. M.; Drake, T. L.; Wu, W.; Lin, Y.; Weitz, E.; Marks, L. D.; Stair, P. C. Highly efficient activation, regeneration, and active site identification of oxide-based olefin metathesis catalysts. *ACS Catal.* **2016**, *6*, 5740−5746.
(53) Andriopoulou, C.; Boghosian, S. Heterogeneity of deposited phases in supported transition metal oxide catalysts: reversible temperature-dependent evolution of molecular structures and configurations. *Phys. Chem. Chem. Phys.* **2018**, *20*, 1742−1751.
(54) Kentri, T.; Trimpalis, A.; Misa, A.; Kordouli, E.; Ramantani, T.; Boghosian, S. Rethinking the molecular structures of $W^{VI}O_x$ sites dispersed on titania: distinct mono-oxo configurations at 430○ C and temperature-dependent transformations. *Dalton Transactions* **2022**, *51*, 7455−7475.
(55) Andriopoulou, C.; Kentri, T.; Boghosian, S. Vibrational spectroscopy of dispersed $Re^{VII}O_x$ sites supported on monoclinic zirconia. *Dalton Transactions* **2024**, *53*, 4020−4034.

https://doi.org/10.1021/acs.jpcc.5c08604
J. Phys. Chem. C 2026, 130, 4096−4108